Instrument Science Report COS 2023-17(v1)

Cycle 29 COS/FUV Spectroscopic Sensitivity Monitor

Kate Rowlands[1], Ravi Sankrit[2]

[1]AURA for ESA, Space Telescope Science Institute, Baltimore, MD
[2]Space Telescope Science Institute, Baltimore, MD

27 June 2023

ABSTRACT

The Cycle 29 COS/FUV spectroscopic sensitivity monitor ran from December 2021 to October 2022. Observations of the G160M modes and G130M/1222 were obtained at Lifetime Position 4 (LP4), the blue modes (G130M/1055 and G130M/1096) were obtained at Lifetime Position 2 (LP2), the G130M standard modes (longwards of cenwave 1222) were obtained at LP5, and the G140L modes were obtained at LP3, starting Oct 4 2021. Connection visits were obtained in preparation for the start of G160M at LP6, and the second pair of LP3 and LP5 connection visits were obtained for G140L and G130M. The Time-Dependent Sensitivity (TDS) slopes of all modes ranged from 0% *to* -3% *per year. In this ISR we describe the program and its execution, and provide a summary of the analysis and results. Based on the change in the net count rates over a one year timescale, and accounting for how a change in HV affects count rates,* we find that the FUV TDS does not depend on LP between LP4 and LP3.

Operated by the Association of Universities for Research in Astronomy, Inc., for the National Aeronautics and Space Administration.

Contents

1. Introduction

The throughput of the COS FUV detector changes with time (Osten et al. 2010), and this is monitored with the COS FUV spectroscopic sensitivity calibration program. Previous programs and their results are detailed in Osten et al. (2011), Bostroem et al. (2015), De Rosa et al. (2016, 2017, 2018), Sankrit (2019, 2020), Sankrit & Rowlands (2021), Rowlands & Sankrit (2022). Sensitivity variations over time are modeled as a function of wavelength for each cenwave and segment (FUVA, FUVB). These are included in the TDS reference file (TDSTAB) for use in CalCOS to obtain flux calibrated data, when paired with the photometric throughput reference file (FLUXTAB).

The Cycle 29 FUV TDS monitor (PID: 16830, PI: K. Rowlands) consisted of observations of the flux calibration standards, GD71 and WD0308-565, with the plan of obtaining data every two months between December 2021 and October 2022. Observations were also performed to check the consistency of the time-dependent sensitivity between LP5 and the previous lifetime position LP4 for G130M/1291–1327, between LP3 and the previous lifetime position LP4 for G140L/800, and between LP6 and the previous default lifetime position LP4 for the G160M modes. LP changes are summarized in Fischer et al. (2022), Plesha et al. (2022) and Sankrit et al. in prep, with details about the LP moves included in Section 2.

2. Program design

The Time-Dependent Sensitivity (TDS) monitoring program observes the bluest and reddest central wavelengths of each grating, with additional coverage of the G130M/1055 and 1096 blue modes, G130M/1222, and the new cenwaves

G160M/1533 and G140L/800 that were added in Cycle 26.

Cenwave G160M/1611 was added in Cycle 29 with the aim of enabling us to disentangle the dependence of the TDS on detector position from its dependence on wavelength. TDS slopes for untracked cenwaves are obtained by averaging individual adjacent tracked cenwave slopes, but it is not clear how well this estimation performs. Monitoring data over the last few cycles showed evidence for sensitivity changes that were detector location dependent (Sankrit & Rowlands 2021). For untracked cenwaves, we do not currently know how to weigh between detector position and wavelength. A third monitored cenwave in between the current ones would allow the separation of wavelength and detector position effects on the TDS, which is likely grating dependent. The TDS slope for cenwave 1611 will be used to assess how well the TDS for this cenwave is tracked by our current averaging method and to find the optimal weights between detector position and wavelength when averaging the TDS slopes of the regularly tracked adjacent cenwaves 1577 and 1623. While some tests can be done with cenwaves 1533, 1577 and 1623, the wavelength overlap is superior with 1577, 1611 and 1623, and the additional cenwave 1611 would allow us to confirm trends seen with cenwaves 1533, 1577 and 1623. The choice of cenwave 1611 was further motivated by being the most used of all G160M cenwaves in Cycle 28, with 8% of all COS exposures.

The white dwarf standard stars WD0308-565 and GD71 have been used for monitoring since Cycle 20, and are currently observed every two months. The modes tracked in Cycle 29 are listed in Tables 1 and 2. The targets for each cenwave and segment are chosen to optimize the signal-to-noise ratio and to minimize the impact on detector lifetime. When GD71 is not observable from mid-April to early August, only WD0308-565 is observed.

Exposure times were determined by requiring a S/N of 15 per resel at the wavelength of least sensitivity for all modes, except the blue modes, G130M/1222, and G140L/800. For the blue modes and for G130M/1222, the goal was to obtain S/N$= 25$ per resel at the wavelength of maximum sensitivity, ensuring S/N> 15 for > 1030Å for G130M/1096/FUVB, and for > 1130Å for G130M/1055/FUVA and G130M/1222. For G140L/800, the target S/N was 15 per resel at the wavelength of least sensitivity longwards of 1150Å, below which there is a sharp drop in throughput. At < 1150Å the exposure time obtains a S/N of 30–40 per 20Å bin.

The exposure times and overheads require two orbits per visit for GD71 and three orbits per visit for WD0308-565. There are no wavelength calibration lamp lines available in the wavelength range covered by G130M/1096/FUVB, so the visits include a GO wavelength calibration lamp observation taken at the same Optics Select Mechanism 1 (OSM1) position immediately after the science exposure using segment FUVA.

The standard mode and new cenwave observations were obtained at the nominal (current) COS FUV lifetime positions (LP4 and LP5), while the blue modes were observed at LP2. COS FUV G130M operations for cenwave 1291 and longwards

Table 1. Modes Tracked using GD71.

Grating	Cenwave	Segment	$t_{\rm exp}$ (sec)
G130M	1096	FUVB[a]	793
G160M	1533	FUVA	106
	1577	FUVA	135
	1611	FUVA	159
	1623	FUVA	177

[a]G130M/1096 is observed with segment FUVB only since the target is too bright to be observed with segment FUVA.

transitioned from LP4 to LP5, and G140L operations transitioned from LP4 to LP3 at the beginning of Cycle 29, on 2021 October 4. G160M operations for all cenwaves moved from LP4 to LP6 as default at the beginning of Cycle 30, on 2022 October 3. Two closely spaced observations of WD0308-565 at LP4 and LP5, and LP4 and LP3 were included as part of the Cycle 28 and 29 programs. Two closely spaced observations of WD0308-565 and GD71 at LP4 and LP6 were were included as part of the Cycle 29 and 30 programs. These connection exposures, taken within the same visit, establish the scaling between the net counts for LP4 and LP6, and were scheduled within 4 weeks from the LP6 visits of the fluxes and flats program (PID 16906, Miller et al. in prep). The LP4–LP5 scaling results are discussed in Rowlands & Sankrit (2022), and the LP4–LP6 scaling results will be discussed in Rowlands & Sankrit (in prep). All observations were obtained at FP-POS $= 3$. The visit structure was unchanged from Cycle 28, except for the addition of the LP3, LP5, and LP6 connection exposures in visits 5A, 5B, 56, 07 and 58 (see Table 3), and the splitting of visit 5 into two (5A and 5B) to aid scheduling.

3. Observations

The data used in the FUV TDS analysis use the observations shown in Table 3, sorted by observation date. The program included eight visits for WD0308-565, and five for GD71, which is not visible between the end of April and the beginning of August. The program was impacted by three failed visits, 03, 06 and 08, on 2022 February 26, 2022 March 21 and 2022 August 20, respectively, and the observations were repeated approximately three weeks later on 2022 March 14 in visit 53, on 2022 April 16 in visit 56, and on 2022 September 14 in visit 58, respectively. All of the data from successful observations are available in the archive.

Table 2. Modes Tracked using WD0308-565.

Grating	Cenwave	Segment	$t_{\rm exp}$ (sec)
G130M	1055	Both	318
	1222	Both	267
	1291	Both	236
	1327[a]	FUVA	274
G160M	1533	FUVB	223
	1577	FUVB	291
	1611	FUVB	360
	1623	FUVB	388
G140L	800[a]	FUVA	367
	1105[a]	FUVA	332
	1280	Both	401

[a]Cenwaves 1327, 800, and 1105 are FUVA-only.

4. Analysis and Results

4.1 Regular TDS monitor

The data were analyzed using the TDS analysis code as described in Bostroem et al. (2015), using calibrated `x1d.fits` files from previous monitoring programs from September 2009–October 2022. Net counts were binned over 20Å for the G140L and blue modes, and over 5Å for the medium resolution modes. With this S/N, we aimed to achieve a flux calibration accuracy of 5% absolute and 2% relative. The data obtained at LP2, LP3, LP4, LP5 and LP6 are scaled to data obtained at LP1, LP2, LP3 and LP4, respectively using the connection observations obtained at the different LPs. Fits to the data using a piecewise-linear function were preformed with breakpoints at decimal years 2010.20, 2011.20, 2011.75, 2012.00, 2012.80, 2013.80, 2015.50, 2019.0 and 2020.60. A new breakpoint at 2020.60 was added so that the TDS model better fit the data. The overall relative sensitivity was normalized to 1.0 at the time of first light (May 01, 2009). Fig 1 shows a summary plot of the sensitivity against time, along with the solar activity towards Earth as a function of time. The 10.7 cm solar fluxes are obtained from the Solar Monitoring Program hosted by Natural Resources Canada at ftp://ftp.seismo.nrcan.gc.ca/spaceweather/solar_flux/daily_flux_values/. Monitoring of the solar flux is important since previous steepenings of the FUV TDS slopes have been correlated with high solar activity (Bostroem et al. 2015). The TDS slopes since 2016 have been stable and typically varied between 0 and -3% per year, and are relatively uniform with wavelength, as shown in Figure 2.

Table 3. Observation dates for PID 16830.

Obs. Date	Visit No.	Target
2021-12-26	02	GD71
2022-01-07	01	WD0308-565
2022-02-18	04	GD71
2022-02-26[$]	03	WD0308-565
2022-03-14	53	WD0308-565
2022-03-21[#$]	06	GD71
2022-04-16[#]	56	GD71
2022-04-16[†]	5B	WD0308-565
2022-04-17[#]	5A	WD0308-565
2022-06-06[†]	07	WD0308-565
2022-08-20[$]	08	WD0308-565
2022-08-20	09	GD71
2022-09-14[⋆]	58	WD0308-565
2022-09-26	12	WD0308-565
2022-09-30	10	WD0308-565
2022-10-16	11	GD71

[#]LP4–LP6 connection visit.

[†]LP4–LP5 connection visit.

[⋆]LP4–LP3 connection visit.

[$]Failed or partially failed visit.

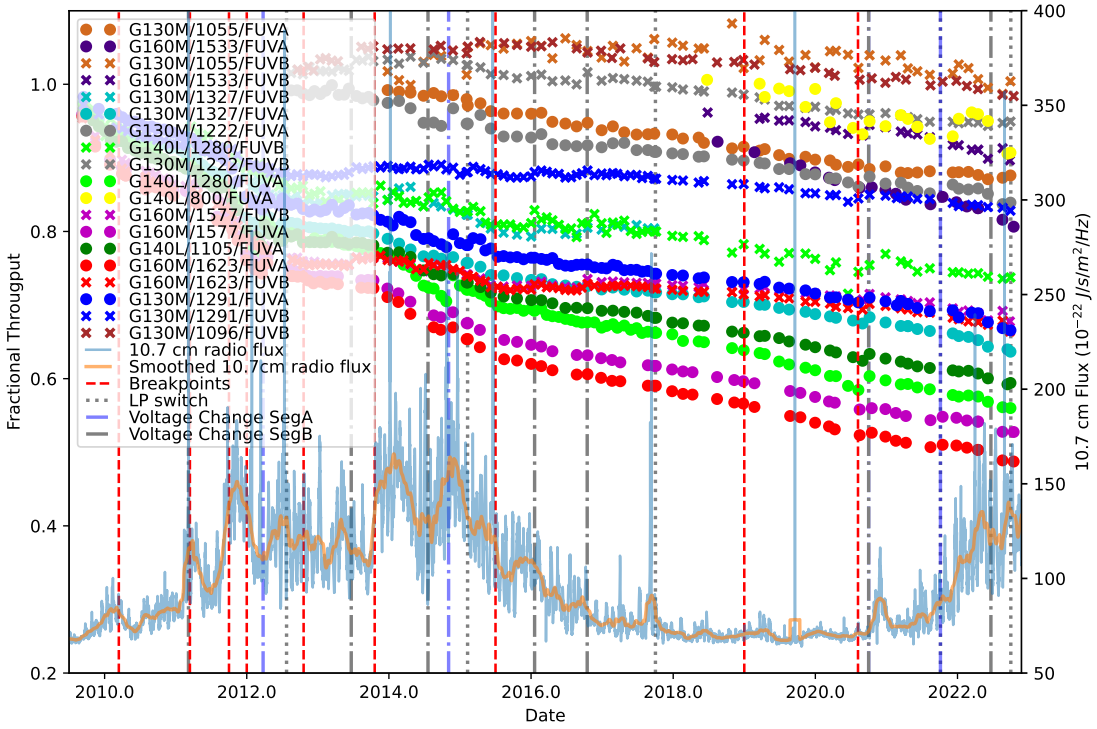

Figure 1. Changing sensitivity as a function of time for monitored COS FUV cenwaves (see legend). The solar flux incident at the Earth is overplotted, and is measured using the 10.7 cm radio flux (blue line: unsmoothed, orange line: smoothed). Dashed red vertical lines are breakpoints in the piece-wise linear function used to model the TDS, dotted grey vertical lines mark the LP moves, and dot-dashed vertical lines correspond to changes in operational voltage.

4.2 LP4–LP3 scaling

The TDS is assumed to be independent of LP, allowing the same TDS model to be applied at all LPs. Similar to LP3–LP4 for all modes (Sankrit 2019), and LP4–LP5 for G130M/1291–1327 (Rowlands & Sankrit 2022), we compare the fractional change in the count rates between two epochs for the G140L/800 cenwave observed at LP3 and LP4. The first epoch observations were obtained as part of the Cycle 28 FUV TDS program (PID 16830), while the second epoch observations were obtained as part of the Cycle 29 FUV TDS program. The dates of the observations and the time intervals between the epochs are listed in Table 4, and the exposures used are listed in Table 5.

The fractional change in the net count rates from the calibrated `x1d.fits` files in % yr^{-1} is calculated as

$$\Delta C(t_1, t_2) = 100. \times ((C_{t_2} - C_{t_1})/C_{t_1}) \times 1/(t_2 - t_1), \quad (1)$$

where C_{t_1} and C_{t_2} are the count rates measured in the Epoch 1 and Epoch 2 data,

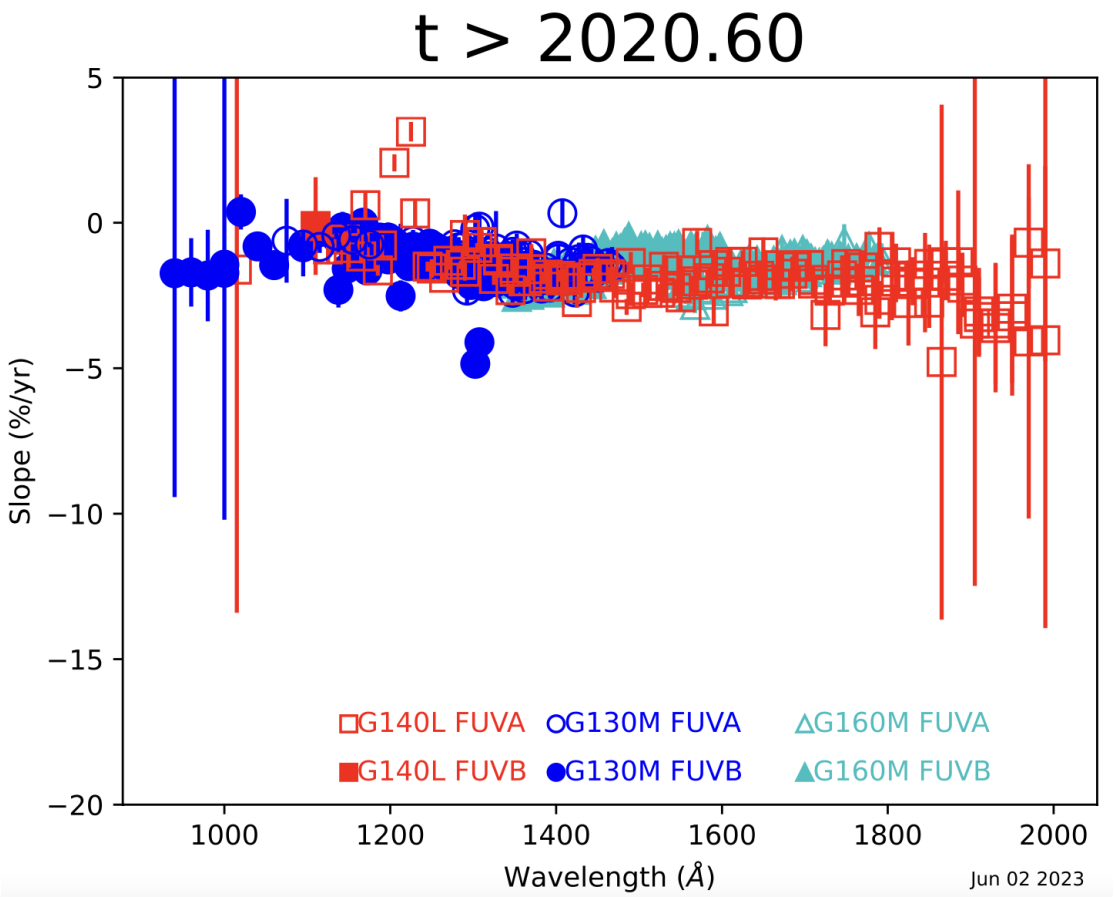

Figure 2. The FUV TDS slopes (percentage change per year) measured during Cycle 29 as a function of wavelength, for each grating and segment (see legend). The FUV TDS slopes were stable during the cycle, and typically varied between 0 and -3% per year. Uncertainties on the slopes are small at most wavelengths, but are larger near the detector edges and around airglow lines.

respectively, and $t_2 - t_1$ is the time interval between the observations in years for each mode (Δt column in Table 4).

We plot the percentage change in net counts for LP4 and LP3 as a function of wavelength, and the difference in these changes in Figure 3 for G140L/800/FUVA. If the TDS is independent of LP then the fractional change in net counts should be similar between LP4 and LP3. The count rates are similar and are typically within 2% of each other, except around detector edges, short wavelengths < 1100Å where the S/N is low, and regions contaminated with airglow lines, where larger differences are seen between the LP4 and LP3 count rates. The count rate differences are typically between 0% and -2%, with an average offset of -1.15% per year. This is because the operating voltage was raised on segment FUVA from 167 to 173 for LP4 on 2021 October 4, which resulted in a change in the net counts. The HV for LP3 was 173 in both epochs.

Table 4. Dates and time intervals for the LP4/LP3 comparison.

Target	LP	Cenwave	Epoch 1	Epoch 2	Δt (yr)	Epoch 1 HV	Epoch 2 HV
WD 0308-565	LP4	800	2021-06-08	2022-09-14	1.27	167	173
WD 0308-565	LP3	800	2021-06-08	2022-09-14	1.27	173	173

[a]Cenwave 800 is FUVA-only, the HV is only reported for segment FUVA.

Table 5. Exposure ROOTNAMEs used for the LP4/LP3 comparison for G140L/800.

Cenwave	Segment	LP4 (epoch 1)	LP4 (epoch 2)	LP3 (epoch 1)	LP3 (epoch 2)
800	FUVA	lefe07lzq	ler158owq	lefe07lxq	ler158oyq

The HV values are summarized in Table 4.

Comparing data before and after the HV raise, the increase in net counts was on average 1% from 1250–1500Å, and was 0% from 1600–1800Å. This was measured from averaging the difference in scaled net counts either side of the HV raise date on segment FUVA for cenwaves that remained at LP4 during the HV raise (G130M/1222 & G160M/1533, G160M/1577 & G160M/1623). The HV change cannot be measured directly from the G140L/800 data, because the HV raise occurred simultaneously with the switch from LP4 to LP3. The difference in scaled net counts either side of the HV raise on LP4 are consistent with those seen in the net count rates between LP3 and LP4 for G140L/800. This slight offset in net counts is consistent with what is observed from previous operating voltage increases. The differences in the count rates are consistent with our tolerance, therefore the TDS does not depend on LP based on LP4 and LP3 data.

5. Continuation Plan

In Cycle 30, the regular monitoring of the FUV TDS continued in program 17249 (PI: K. Rowlands). The targets and frequency of visits are the same as in Cycle 29. Additional observations are planned to support the flux calibration of G160M that will start at LP6 in Cycle 30. Additionally, we will continue to monitor cenwave G160M/1611 to help disentangle the dependence of the TDS on detector position from its dependence on wavelength. The TDS slope shown by cenwave 1611 will be used to find the optimal weights between detector position and wavelength when averaging the TDS slopes of

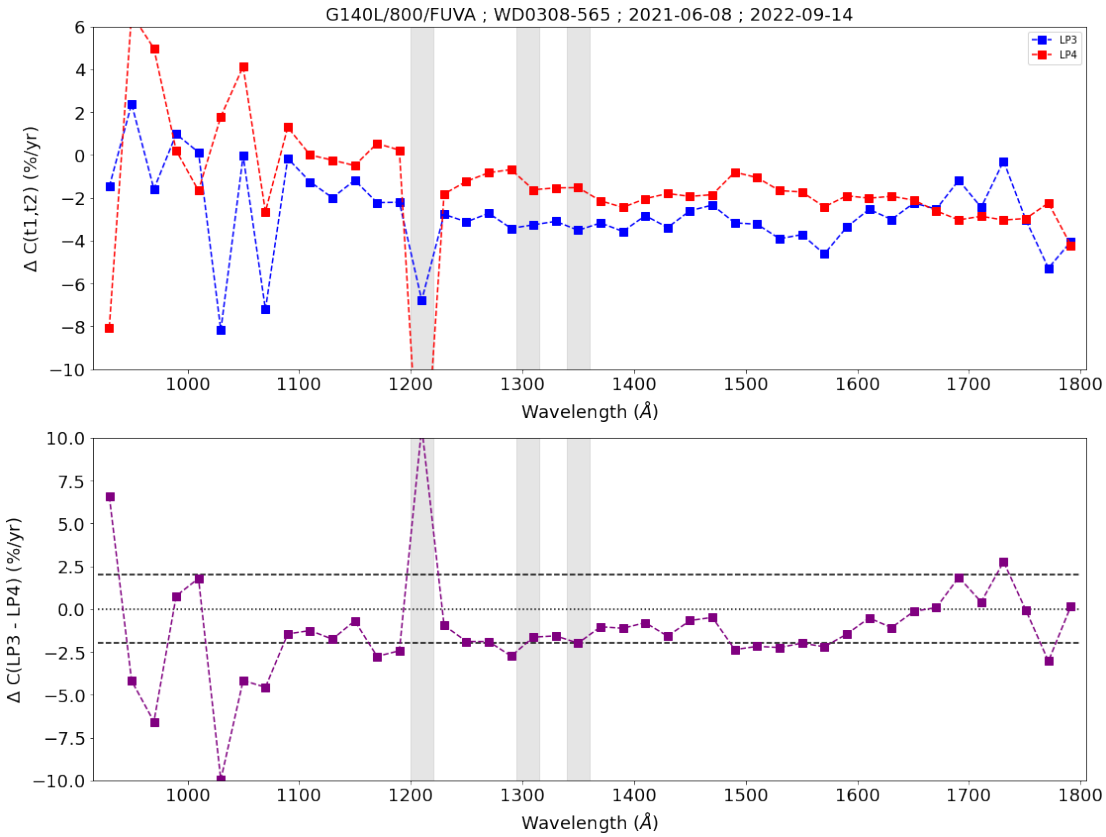

Figure 3. Results for G140L/800, segment FUVA. Top panel: Changes in the net count rates at LP3 (blue squares) and LP4 (red squares), in % yr^{-1}, in 20Å bins. The grey shaded regions show wavelength ranges contaminated with airglow lines. The bottom panel shows the difference between the LP3 and LP4 net count rates also in % yr^{-1}.

the regularly tracked cenwaves 1577 and 1623.

Change History for COS ISR 2023-17

Version 1: 27 June 2023- Original Document

References

Bostroem, K. A., et al. 2015, COS Technical Instrument Report 2014-05
De Rosa, G., Sana, H., Ely, J. and the COS team, 2016, COS Instrument Science Report 2016-13
De Rosa, G. and the COS team, 2017, COS Instrument Science Report 2017-10
De Rosa, G. and the COS team, 2018, COS Instrument Science Report 2018-09
Fischer, W. J. et al., 2022, COS Instrument Science Report 2022-03
Oliveira, C., et al. 2018, COS Instrument Science Report 2018-16
Osten, R. A., et al. 2010, COS Instrument Science Report 2010-15

Osten, R. A., et al. 2011, COS Instrument Science Report 2011-02
Plesha, R., et al. 2022, COS Technical Instrument Report 2022-03
Sankrit, R. 2019, COS Instrument Science Report 2019-18
Sankrit, R. 2020, COS Instrument Science Report 2020-06
Sankrit, R. & Rowlands, K., 2021, COS Instrument Science Report 2021-02
Rowlands, K. & Sankrit, R., 2022, COS Instrument Science Report 2022-08